




## Open Archive Toulouse Archive Ouverte (OATAO)

OATAO is an open access repository that collects the work of Toulouse researchers and makes it freely available over the web where possible

This is an author's version published in: <http://oatao.univ-toulouse.fr/21403>

**Official URL:** <https://doi.org/10.1016/j.jallcom.2018.04.302>

**To cite this version:**

Maury, Nicolas and Denand, Benoît and Dehmas, Moukrane  and Archambeau-Mirguet, Claude and Delfosse, Jérôme and Aeby-Gautier, Elisabeth *Influence of the ageing conditions and the initial microstructure on the precipitation of  $\alpha$  phase in Ti-17 alloy*. (2018) *Journal of Alloys and Compounds*, 763. 446-458. ISSN 0925-8388

Any correspondence concerning this service should be sent to the repository administrator: [tech-oatao@listes-diff.inp-toulouse.fr](mailto:tech-oatao@listes-diff.inp-toulouse.fr)

# Influence of the ageing conditions and the initial microstructure on the precipitation of $\alpha$ phase in Ti-17 alloy

Nicolas Maury<sup>a, b, \*</sup>, Benoît Denand<sup>a, c</sup>, Moukrane Dehmas<sup>a, c, d</sup>,  
Claude Archambeau-Mirguet<sup>b</sup>, Jérôme Delfosse<sup>e</sup>, Elisabeth Aeby-Gautier<sup>a, c</sup>

<sup>a</sup> Université de Lorraine, CNRS, IJL, F-54000 Nancy, France

<sup>b</sup> Airbus Operations S.A.S., 316 route de Bayonne, 31060 Toulouse, France

<sup>c</sup> Laboratory of EXcellence Design of Alloy Metals for Low-mAss Structures ("DAMAS" Labex), Université de Lorraine, France

<sup>d</sup> CIRIMAT, Université de Toulouse, 4 allée Emile Monso, 31030 Toulouse, France

<sup>e</sup> Airbus Group S.A.S., Airbus Group Innovations, 12 rue Pasteur, 92152 Suresnes, France

## ARTICLE INFO

### Keywords:

Metals and alloys  
Phase transitions  
Crystal structure  
Microstructure  
X-ray diffraction

## ABSTRACT

The precipitation of  $\alpha$  phase during ageing was investigated in the near- $\beta$  titanium alloy Ti-17 considering either a fully  $\beta_{\text{metastable}}$  initial microstructure or a 35%  $\alpha_{\text{primary}}$  + 65%  $\beta_{\text{metastable}}$  initial microstructure. In-situ electrical resistivity and high energy X-ray diffraction measurements revealed the influence of the initial microstructure, with different  $\alpha$  morphologies (size and distribution of  $\alpha_{\text{primary}}$ ), as well as the heating rate on the precipitation sequences and kinetics following the decomposition of the  $\beta$ -metastable phase. Various amounts of metastable phases ( $\omega_{\text{isothermal}}$  and  $\alpha''_{\text{isothermal}}$ ) precipitate in temperature ranges that increase with the heating rate. From temperatures about 500 °C, the orthorhombic  $\alpha''_{\text{isothermal}}$  structure evolved towards the hexagonal close-packed  $\alpha$  as temperature increased. SEM microstructure characterisations showed that slow heating rates promoted a fine and dense  $\alpha$  precipitate distribution through the formation of  $\omega_{\text{isothermal}}$  and/or  $\alpha''_{\text{isothermal}}$ , leading to higher hardness values. A higher heating rate restricted the precipitation of  $\alpha''_{\text{isothermal}}$  and shifted to the one of  $\alpha$  at a higher temperature, leading to coarser precipitates. Furthermore, precipitation kinetics of  $\alpha''_{\text{isothermal}}/\alpha$  were quicker considering an initial intragranular  $\alpha$  precipitation as compared to  $\alpha$  colonies.

## 1. Introduction

Titanium-based alloys provide a very good combination of high specific strength and excellent corrosion resistance which results in a wide range of aerospace applications such as the manufacturing of engine blades, landing gears or pylons [1–3]. In the aeronautical industry in particular, new environmental targets require weight reductions in structural parts, resulting in the increasing use of these alloys in substitution of stainless steels and nickel-based alloys. As a result of improved engine performances, these parts are exposed to higher operating temperatures that question the microstructural evolutions of near- $\beta$  alloys, including Ti-17. This class of titanium alloys has been of much interest in the recent past due the refinement of microstructures as compared to more

commonly used  $\alpha/\beta$  alloys. This refinement exhibits a much higher strength [4] due to a fine scale distribution of  $\alpha$  precipitates in the  $\beta$  matrix, associated with a high density of  $\alpha/\beta$  interfaces [5]. The formation of such microstructures requires the control of the thermal paths and in particular the ageing stage.

A better understanding of the variability in mechanical properties in large parts manufactured with near- $\beta$  alloys due to ageing processes is therefore needed. These properties vary with the microstructural parameters of the  $\alpha$  phase precipitates (morphology, density, size, spatial distribution and volume fraction) as a consequence of the various heating rates within the part. The final microstructural parameters are strongly influenced by the sequences and kinetics of phase transformations during thermal treatments [6,7]. Many contributions have focused on the decomposition kinetics of the  $\beta_{\text{metastable}}$  phase during ageing for several alloys (VT22 [8],  $\beta\text{Cez}$  [9], Ti-LCB [10], Ti-17 [11], Ti-5553 [12,13], Ti-5553-1Zr [14] and also Ti-B19 [15]). In most cases, the initial microstructure was fully  $\beta_{\text{metastable}}$ . The authors reported during heating with low rates the formation of several metastable phases

\* Corresponding author. Université de Lorraine, CNRS, IJL, F-54000 Nancy, France.  
E-mail addresses: nicolas.maury@univ-lorraine.fr, nicolas.n.maury@airbus.com  
(N. Maury).

( $\omega_{\text{isothermal}}$  and  $\alpha''_{\text{isothermal}}$ <sup>1</sup>), depending on the annealing conditions, which strongly affected the final microstructure consisting of a mixture of  $\alpha + \beta$ .

Much less attention was given up to now to initial  $\alpha_{\text{primary}} + \beta_{\text{metastable}}$  microstructures for a same ageing condition. The resulting bimodal microstructures consist in the initial primary  $\alpha$  precipitates and additional  $\alpha$  precipitates that formed during the ageing treatment.  $\beta$  phase is also remaining. For a similar amount of  $\beta$  phase, it was shown that the additional precipitates gather strength, while the initial ones maintain a good level of ductility as compared to fully  $\beta_{\text{metastable}}$  transformed microstructures [17–20].

Indeed, for a Ti-5553 alloy submitted to an ageing treatment of 2 h at 620 °C from a 100%  $\beta_{\text{metastable}}$  microstructure (heating rate of 0.1 °C s<sup>-1</sup>), Settefrati [18] obtained an ultimate tensile strength of 1461 MPa, as well as a strain at failure of 0.2%. The same ageing condition from an initial microstructure 15%  $\alpha_{\text{primary}} + 85\%$   $\beta_{\text{metastable}}$  led to a yield strength (at 0.2% plastic strain) of 1276 MPa, an ultimate tensile strength of 1302 MPa, but also a strain at failure of 2.3%. In both cases, the final total  $\alpha$  phase amount was similar. In another study on Ti-17 alloy, Aeby-Gautier et al. [17] show that the presence of additional  $\alpha$  precipitates formed during ageing increases the yield strength and ultimate tensile strength, while the strain at failure decreases. Bimodal microstructures resulting from an initial  $\alpha_{\text{primary}} + \beta_{\text{metastable}}$  microstructure thus improve the strength–ductility trade-off after ageing and are of growing interest. For this type of initial microstructure, past works on Ti-5553 [12] and Ti-18 [21] alloys highlighted the sensitivity of the precipitation kinetics during ageing to the chemical composition of the  $\beta_{\text{metastable}}$  phase.

This latter point is further investigated in the present study on Ti-17 alloy with an initial microstructure consisting of either about 35%  $\alpha_{\text{primary}} + 65\%$   $\beta_{\text{metastable}}$  (vol. %) or fully  $\beta_{\text{metastable}}$ . The influence of the heating rate and the initial microstructure (fully  $\beta_{\text{metastable}}$  or with different  $\alpha$  morphologies) on the precipitation sequences and kinetics of  $\alpha$  phase during ageing have been determined by means of in-situ high energy synchrotron X-ray diffraction and in-situ electrical resistivity measurements, complemented by microstructural characterisations and hardness measurements as first measures of the mechanical properties.

## 2. Material and experimental procedure

### 2.1. Material

The chemical composition of the Ti-17 alloy investigated is given in Table 1. The  $\beta$  transus temperature ( $T_{\beta}$ ) was found to be 890 °C by electrical resistivity measurements. Samples were cut from the same radius of the received billet, in order to avoid variations in texture, and machined into cylindrical specimens of different sizes: 4.0 mm in diameter x 30.0 mm in length for electrical resistivity measurements and 3–5.5 mm in diameter x 15.0 mm in length for high-energy X-ray diffraction.

### 2.2. In-situ characterisation of phase transformations

#### 2.2.1. Electrical resistivity measurement

In-situ electrical resistivity experiments were undertaken on a self-designed dilatometer to track the phase transformation kinetics during controlled heat treatments inside a radiant furnace, as previously carried out on titanium alloys [6,9,22]. A “four points”

**Table 1**  
Chemical composition of the Ti-17 alloy used in this study.

Element	Ti	Al	Mo	Cr	Sn	Zr	O
Wt.%	Balance	5.1	3.9	3.9	2.1	2.0	0.2

method was used with a continuous current of 2A and the resulting potential difference was recorded and amplified [23]. The temperature, measured by a (S-type) thermocouple spot-welded on the surface of the specimen, was monitored and controlled using a numerical PID regulator. All experiments were carried out under vacuum ( $\approx 10^{-4}$  mbar) in order to limit the oxidation of the samples.

#### 2.2.2. Time resolved high energy X-ray diffraction

In-situ high energy X-ray diffraction (HEXRD) was used to identify the precipitation sequences and their kinetics. Experiments were conducted at the ESRF (European Synchrotron Radiation Facility) in Grenoble (France), on the ID15B beam-line with a monochromatic beam of about 87 keV and a beam size of 400  $\mu\text{m} \times 400 \mu\text{m}$ . The wavelength ( $\lambda = 0.014245$  nm) was calibrated using a standard powder of CeO<sub>2</sub>. A detailed description of the experimental procedure can be found in Ref. [24]. The experimental device consisted of a radiant furnace to apply the controlled heat treatment. A rotating sample holder was used to increase the diffraction volume, and therefore have a good counting statistics and limit any texture effect. More importantly, this rotating equipment was also designed the control of the temperature by spot-welding a (S-type) thermocouple on the specimen. It was placed under a quartz bell-jar with a constant 99.9% pure argon gas flow to minimise the oxidation of the surface. The Debye-Scherrer patterns were collected by a Perkin Elmer detector with a 200  $\mu\text{m} \times 200 \mu\text{m}$  pixel size and an exposure time of 1 s. The Intensity-2 $\theta$  diffraction patterns were then characterized by the Rietveld method [25] on the FullProf software [26], after circular integration of the intensity along the Debye-Scherrer rings using the Fit2D software [27]. The resulting Rietveld refinements give the mean cell parameters and phase weight fractions. These fractions are then converted into volume fractions, considering the phase volumetric mass density at each temperature.

Post-mortem characterisations at room temperature were also carried out on aged samples at the Deutsches Elektronen Synchrotron facility (DESY) in Hamburg (Germany) in order to determine the  $\alpha$  phase volume fraction following each ageing treatments. The experiments took place on the PETRA III station (P07 beamline) with similar conditions as mentioned above ( $\lambda = 0.01424$  nm) and a beam size of 800  $\mu\text{m} \times 800 \mu\text{m}$ . A standard LaB<sub>6</sub> powder was used for calibration. Image sequences were recorded using a Perkin Elmer detector with an acquisition time of 0.1 s and then analyzed by the methodology described above.

### 2.3. Microstructural characterisations

The final aged microstructures were characterized using a scanning electron microscope (SEM) Philips XL30 field emission gun in backscattered electron mode (BSE), operated at an acceleration voltage of 15 kV. About 1500 SEM-BSE images were automatically acquired without prior etching of the sample and then analyzed in order to quantify phase fractions. The surface fraction is equal to the volume fraction whatever the morphology of the precipitates, when the number of analyzed images is sufficient [28]. An image processing routine was developed on the Aphelion™ Dev software [29]. An example is given in Fig. 1 to quantify the volume fraction of the coarse  $\alpha$  lamellar precipitates. The strong contrast in

<sup>1</sup> Following Bönisch [16], the term  $\alpha''_{\text{isothermal}}$  is used to differentiate the orthorhombic structure formed during heating or isothermal holding from the one formed during quenching (i.e.  $\alpha'$  martensite).

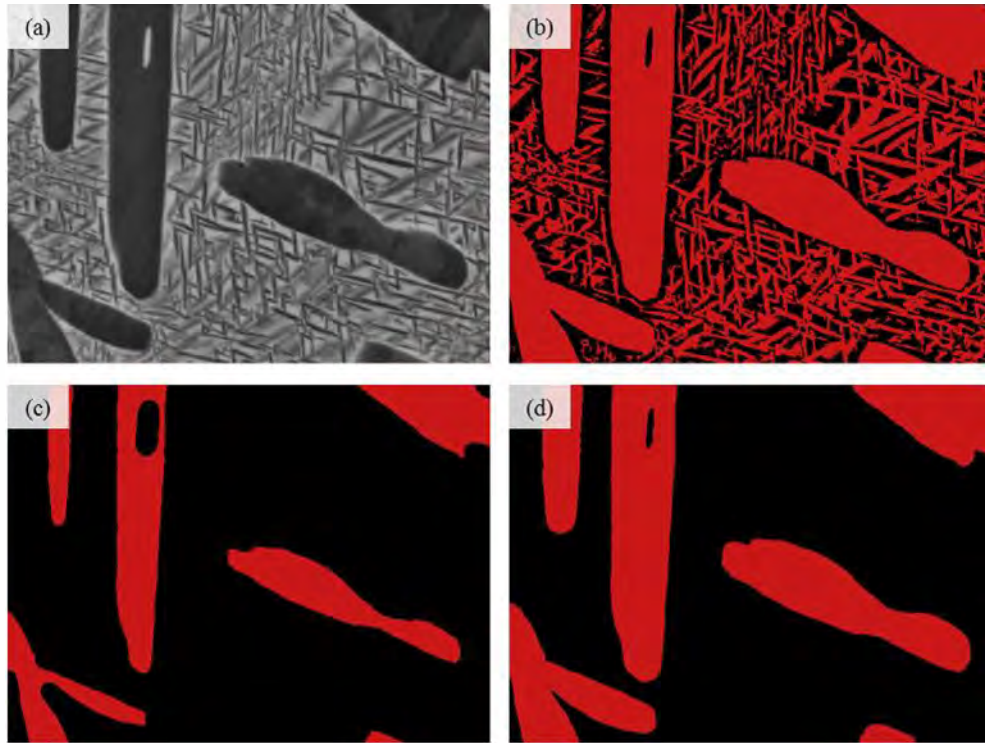


**Fig. 1.** Image analysis process routine to quantify the fraction of the  $\alpha$  coarse precipitates: (a) initial SEM-BSE image, (b) threshold, (c) erosion and (d) dilatation of the binary image with the same disc structuring element.

the SEM-BSE image enables to distinguish the  $\alpha$  phase from the  $\beta$  phase (Fig. 1(a)). First of all, a threshold of the  $\alpha$  phase is performed. This produces a binary image (Fig. 1(b)) which is then eroded using a disc structuring element to clear the background noise and the smaller  $\alpha$  precipitates formed during ageing (Fig. 1(c)). A final morphological dilatation with the same disc structuring element enables to retrieve the shape and size of the coarse  $\alpha$  precipitates (Fig. 1(d)). The fraction is then quantified from this latter image.

Finer scale microstructural characterisations were carried out on thin foils prepared using a FEI Helios NanoLab 600i DualBeam equipped with the Focused Ion Beam (FIB) technique. Selected area electron diffraction patterns and dark-field images were then acquired on a transmission electron microscope (TEM) Philips CM200 operated at 200 kV.

#### 2.4. Thermal treatments and initial microstructures

Complex heat treatments were performed in order to obtain bi-modal microstructures, as illustrated in Fig. 2. They consisted of two steps that will be referred to as “initial heat treatment” followed by “ageing”. These two annealing treatments led to the formation at first of “primary  $\alpha$  phase” ( $\alpha_{\text{lam-primary}}$ ) followed by “secondary  $\alpha$  phase” ( $\alpha_{\text{secondary}}$ ). As only thermal treatments were performed in this investigation (no mechanical deformation), the morphology of the  $\alpha$  precipitates formed during the initial treatment is lamellar, hence the terminology  $\alpha_{\text{lam-primary}}$  used in the following to designate these lamellae formed before ageing in the  $\beta$  grains or at the  $\beta/\beta$  grain boundaries. The term “primary” thus refers only to the  $\alpha$  phase formed during the initial heat treatment (prior to ageing).

Specimens submitted to these initial heat treatments were first all annealed at 920 °C for 15 min, in the  $\beta$  phase field. This solution treatment ensured a fully homogeneous microstructure with an average  $\beta$  grain size of  $\approx 1500 \mu\text{m}$ . The “100%  $\beta_{\text{m}}$ ” initial heat treatment was obtained by immediate quenching to room

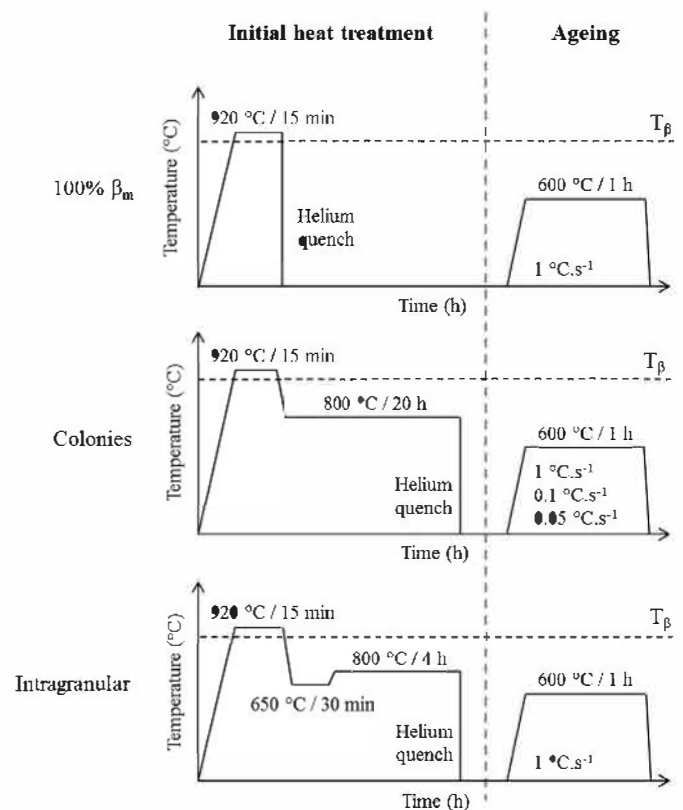


**Fig. 2.** Schematic illustration of the two-step annealing heat treatments performed: “100%  $\beta_{\text{m}}$ ”, “Colonies” and “Intragranular” initial heat treatments followed by ageing at 600 °C for 1 h.

temperature by blowing helium gas, leading to a 100%  $\beta_{\text{metastable}}$  initial microstructure. The resulting microstructure (Fig. 3(a)) shows the coarse  $\beta$  phase grains without any  $\alpha$  precipitates. For “Colonies” and “Intragranular” initial heat treatments, after cooling ( $\approx 4^\circ\text{C s}^{-1}$ ) from 920 °C, isothermal holdings were performed in the ( $\alpha + \beta$ ) phase field in order to precipitate various  $\alpha_{\text{lam-primary}}$  morphologies (different precipitate sizes and spatial distributions) as shown in previous studies [7] [30]. For these two cases, the dwell at 800 °C was selected to obtain a similar  $\alpha$  phase amount of  $\approx 35 \text{ vol.}\%$  [30]. The microstructure was then frozen during quenching at room temperature by blowing helium gas (cooling rate above  $4^\circ\text{C s}^{-1}$  down to 100 °C).

During type “Colonies” initial heat treatment, an isothermal holding at 800 °C for 20 h was performed. At this temperature, grain boundary  $\alpha$  layers ( $\alpha_{\text{GB}}$ ) nucleate and grow first along the  $\beta/\beta$  grain boundaries. Colonies of Widmanstätten parallel sideplates ( $\alpha_{\text{WGB}}$ ) with the same variant then grow from these layers towards the center of the  $\beta$  grains until a hard impingement is reached [7,31]. The resulting initial microstructure is shown in Fig. 3(b). The  $\alpha$  precipitates formed, which appear in dark, exhibit a lamellar morphology resulting from the thermal treatment; they are referred to as  $\alpha_{\text{lam-primary}}$ . The average length and width of these lamellae are 12.8  $\mu\text{m}$  and 2.05  $\mu\text{m}$  respectively. It is worth mentioning that some may appear more discrete due to the apparent two dimensional observation of the morphology the  $\alpha_{\text{lam-primary}}$  precipitates [31]. The corresponding volume fraction of  $\alpha$  phase ( $\alpha_{\text{GB}} + \alpha_{\text{WGB}}$ ) was found to be 32 ( $\pm 2$ )% by Rietveld refinement from X-ray diffraction and 35 ( $\pm 2$ )% by image analysis without etching of the sample. The difference in the fractions determined by both techniques is linked to uncertainties which are difficult to quantify because numerous factors are involved. However, they have been used with uncertainties of less than or equal to 2%.

In the case of the type “Intragranular” initial heat treatment, the

specimen was first isothermally held at 650 °C for 30 min in order to favour intragranular nucleation, leading to the plate morphology named  $\alpha_{\text{WI}}$  (standing for Widmanstätten Intragranular). The following reheating at 800 °C enabled to reach an  $\alpha$  phase amount close to the one obtained after type “Colonies” initial heat treatment, before performing the ageing treatment. Fig. 3(c) shows the resulting microstructure. Compared to the previous type, the precipitation density is higher and the length and width of the lamellar precipitates are significantly reduced. Also, their spatial distribution reproduces a distinct basket-weave pattern with a reduced inter-lamellar gap as shown in Fig. 3(d) at a finer scale. Their volume fraction ( $\alpha_{\text{GB}} + \alpha_{\text{WGB}} + \alpha_{\text{WI}}$ ) after quenching to room temperature was measured at 36 ( $\pm 2$ )% by Rietveld refinement from X-ray diffraction and 31 ( $\pm 2$ )% by image analysis. By comparison, the  $\alpha$  volume fraction predicted by calculation on the Thermo-Calc<sup>®</sup> software, using the titanium alloys TTT13 database [32] and the chemical composition given in Table 1, is 38% at 800 °C. Both “Intragranular” and “Colonies” initial microstructures are thus close to equilibrium.

Fig. 4(a) shows the electron diffraction pattern acquired in the  $\beta_{\text{metastable}}$  phase after type “Colonies” initial heat treatment (i.e. after quenching from 800 °C). Typical diffraction spots corresponding to two variants of the  $\omega_{\text{athermal}}$  phase are observed. These spots are partially connected by diffuse scattering. A similar diffraction pattern denoting the presence of  $\omega_{\text{athermal}}$  was obtained following type “Intragranular” initial heat treatment (Fig. 4(c)). Corresponding dark field images on these  $\omega_{\text{athermal}}$  spots show very fine precipitates, of few nanometers in size and in high density, for both conditions (Fig. 4(b) and (d)). No TEM characterisation for the “100%  $\beta_{\text{m}}$ ” initial state was performed, as it has already been reported several times in previous works the presence of the  $\omega_{\text{athermal}}$  phase following quenching to room temperature [33–35].

Following these three different types of initial heat treatments, all specimens were aged at the temperature of 600 °C for one hour.

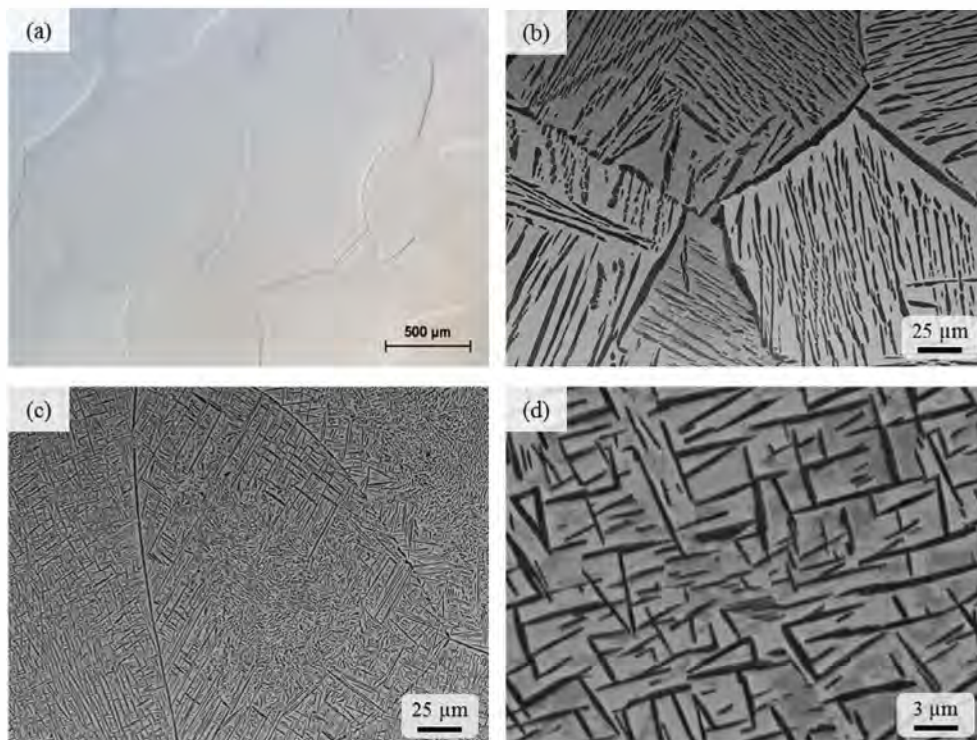
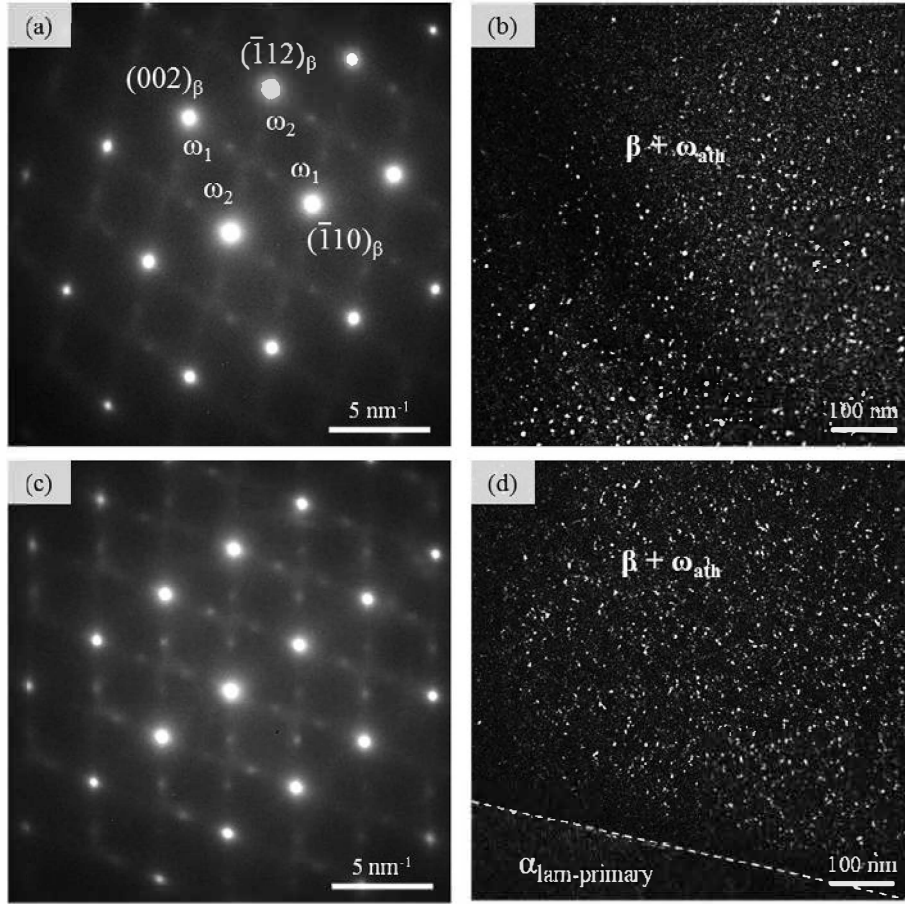


Fig. 3. SEM observation of the initial microstructure resulting from type (a) “100%  $\beta_{\text{m}}$ ” (optical micrography), (b) “Colonies” and (c)–(d) “Intragranular” initial heat treatment.



**Fig. 4.** TEM observation following type "Colonies" and "Intragranular" initial heat treatments: (a) and (c) selected area electron diffraction patterns with a  $[110]_{\beta}$  zone axis, (b) and (d) dark-field images of  $\omega_{\text{athermal}}$  nano-scale precipitates.

The influence of the heating rate on the final precipitation state of  $\alpha_{\text{secondary}}$  was investigated considering type "Colonies" initial heat treatment, for heating rates of  $1^{\circ}\text{C s}^{-1}$ ,  $0.1^{\circ}\text{C s}^{-1}$  and  $0.05^{\circ}\text{C s}^{-1}$ . Moreover, the influence of the initial  $\alpha_{\text{lam-primary}}$  microstructure for all three initial heat treatments was analyzed considering one heating rate of  $1^{\circ}\text{C s}^{-1}$ .

### 3. Results

#### 3.1. Influence of the heating rate

The size and density of  $\alpha_{\text{secondary}}$  precipitates formed during ageing is strongly influenced by the heating rate up to the ageing temperature. This effect is related to the temperature evolution and the precipitation kinetics.

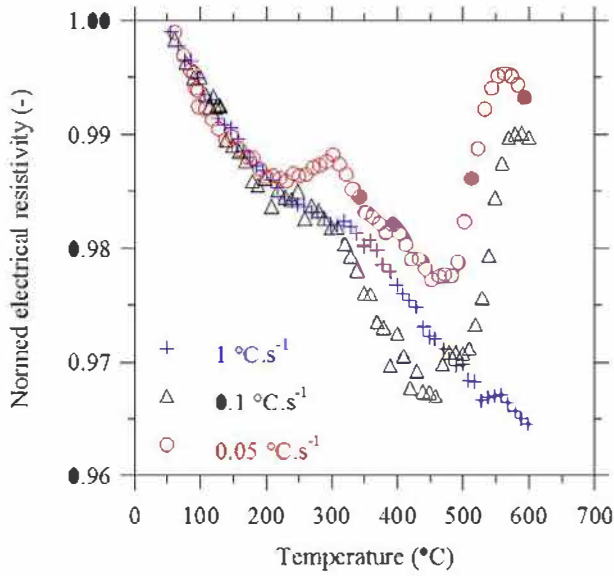
The evolution of the electrical resistivity (normed by the electrical resistivity at room temperature) during heating up to  $600^{\circ}\text{C}$  for the three heating rates of  $1^{\circ}\text{C s}^{-1}$ ,  $0.1^{\circ}\text{C s}^{-1}$  and  $0.05^{\circ}\text{C s}^{-1}$ , from type "Colonies" initial heat treatment, is reported in Fig. 5(a). Starting at room temperature, the electrical resistivity decreases with a similar trend when heating, whatever the rate. All three curves then show a non-linear behavior with an increase in their slope between  $200^{\circ}\text{C}$  and  $310^{\circ}\text{C}$ , reaching even a positive value for the lowest heating rate ( $0.05^{\circ}\text{C s}^{-1}$ ).

As heating continues above  $310^{\circ}\text{C}$ , the electrical resistivity decreases again with different slopes of the curves in a temperature range varying with the heating rate. For the rate of  $1^{\circ}\text{C s}^{-1}$ , the decrease is continuous until the ageing temperature. However,

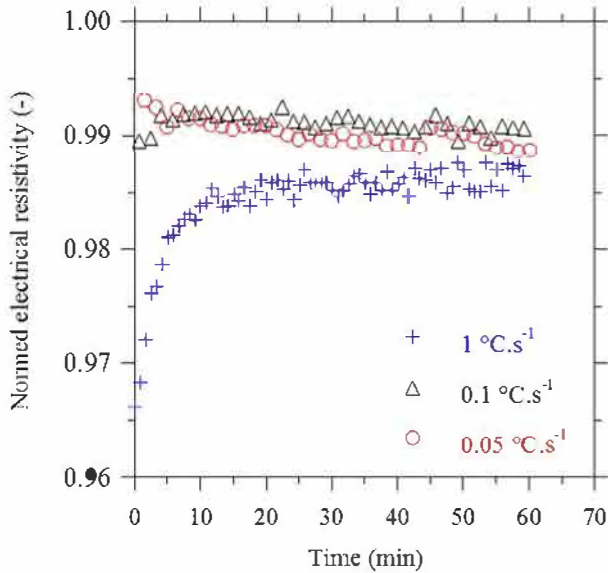
when the isothermal holding at  $600^{\circ}\text{C}$  begins, there is a sharp increase in electrical resistivity during 15 min followed by a stabilization to a value which tends towards the one for the two other heating rates (Fig. 5(b)). For the intermediate rate of  $0.1^{\circ}\text{C s}^{-1}$ , on the contrary, the electrical resistivity increases significantly between  $460^{\circ}\text{C}$  and  $580^{\circ}\text{C}$  before stabilizing during the isothermal holding at  $600^{\circ}\text{C}$ . Finally, for the lowest heating rate ( $0.05^{\circ}\text{C s}^{-1}$ ), there is also an increase between  $480^{\circ}\text{C}$  and  $570^{\circ}\text{C}$ , with an amplitude less important than for the rate of  $0.1^{\circ}\text{C s}^{-1}$  but up to the highest normed value. The electrical resistivity then starts to decrease from  $570^{\circ}\text{C}$  and also during the dwell at  $600^{\circ}\text{C}$ . At the end of the holding time, the three normed values are quite similar, regardless of the heating rate.

Based on previous studies, the variations in electrical resistivity are associated with phase transformations leading to precipitation in the  $\beta_{\text{metastable}}$  phase. These will be detailed and discussed in comparison with the present investigation hereafter (section 4).

Structural evolutions during the heating stage have been characterized by in-situ HEXRD. Fig. 6 shows some diffraction patterns ( $I, 2\theta$ ) recorded while heating at the rate of  $0.1^{\circ}\text{C s}^{-1}$ . The angular domain has been restricted between  $4.4^{\circ}$  and  $5.8^{\circ}$ , which takes into account the peaks  $\{10\bar{1}2\}_{\alpha}$ ,  $(200)_{\beta}$  and  $\{11\bar{2}0\}_{\alpha}$  at room temperature at the positions  $2\theta = 4.74^{\circ}$ ,  $2\theta = 5.03^{\circ}$  and  $2\theta = 5.58^{\circ}$ . Despite the change of slope of electrical resistivity during heating, no significant evolution could be observed between room temperature and  $300^{\circ}\text{C}$ , except a slight displacement of the diffraction peaks due to thermal expansion (the top of the  $\alpha$  and  $\beta$  peaks has been cut for an easier observation).



(a)



(b)

**Fig. 5.** Evolution of the normed electrical resistivity when performing ageing at 600 °C following type “Colonies” initial heat treatment: (a) during heating for three different rates and (b) during the one-hour isothermal holding.

Between 490 °C and 520 °C, shoulders appear on the side of the  $\{10\bar{1}2\}_\alpha$  and  $\{11\bar{2}0\}_\alpha$  initial peaks. These shoulders, clearly revealed in Fig. 7 in this temperature domain, have been identified as the characteristic peaks of an orthorhombic structure (diffraction peaks  $(022)_{\alpha''}$  and  $(200)_{\alpha''}$ ), highlighting the precipitation of the  $\alpha''_{\text{isothermal}}$  metastable phase during heating. The crystallographic structures of the  $\alpha$ ,  $\beta$  and  $\alpha''$  phases used for identification are reported in Table 2 (the y coordinate for  $\alpha''_{\text{isothermal}}$  was defined at 0.2 [36] and is very close to the ones determined by Rietveld refinement in previous works on Ti-10V-2Fe-3Al [37], Ti-24Nb-4Zr-8Sn [38] and Ti-Nb alloys [39]). In the angular domain studied, the base centered (called  $\alpha''$ ) [36,40] or the ordered face centered (called  $O''$ ) [41] orthorhombic structures can be considered. For further characterisations, the more commonly reported structure

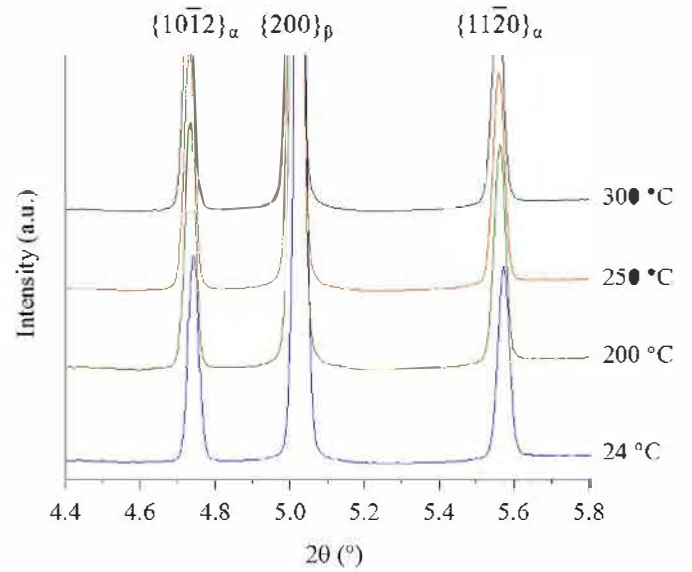


**Fig. 6.** Evolution of synchrotron X-ray diffraction patterns acquired during heating at a rate of 0.1 °C s<sup>-1</sup>, after type “Colonies” initial heat treatment, from room temperature to 300 °C.

(base centered orthorhombic) was chosen.

The intensity of the  $\alpha''_{\text{isothermal}}$  shoulders is maximum at 520 °C, and at the same time the intensity of the  $\beta$  peak decreases considerably while for the two  $\alpha$  peaks it increases gradually. From above 520 °C, the  $\alpha''_{\text{isothermal}}$  shoulders gradually disappear and the two  $\{10\bar{1}2\}_\alpha$  ( $2\theta = 4.72^\circ$ ) and  $\{11\bar{2}0\}_\alpha$  ( $2\theta = 5.54^\circ$ )  $\alpha$  peaks narrow and gain intensity when the temperature increases. This in-situ HEXRD experiment thus reveals that microstructural evolutions occurred from 490 °C up to the ageing temperature, temperature domain corresponding to the notable increase in electrical resistivity when heating at 0.1 °C s<sup>-1</sup> (Fig. 5(a)).

The final microstructures obtained after ageing treatment for the three heating rates, from type “Colonies” initial heat treatment, are shown in Fig. 8. A clear bi-modal microstructure is observed for all heating conditions, with the initial  $\alpha_{\text{lam-primary}}$  lamellae and the  $\alpha_{\text{secondary}}$  plates formed in the  $\beta$  matrix during the ageing treatment. The  $\alpha_{\text{lam-primary}}$  fractions quantified by image analysis range between 34% and 35% for the three heating conditions as summarized in Table 3. These are close to the ones determined after the initial heat treatments. It can thus be considered that the ageing treatment at 600 °C did not lead to notable changes in the amount and size of these coarse lamellae previously formed at 800 °C.

The total amount of  $\alpha$  phase, characterized by HEXRD, is also given in Table 3 for each condition. At the end of the one-hour ageing, the total  $\alpha$  volume fraction is very close (57%–58%) whatever the heating rate. The fraction of  $\alpha_{\text{secondary}}$  plates can thus be deduced by subtracting the  $\alpha_{\text{lam-primary}}$  fraction determined by image analysis to the total amount of  $\alpha$ . This amount is nearly identical for all three conditions (22%–23% of  $\alpha_{\text{secondary}}$  plates), considering some deviations for each experimental technique.

Focusing on the  $\alpha_{\text{secondary}}$  plates, significant differences in the size and precipitation density can be noticed in these microstructures. Their number density is the highest and their size is the smallest for the heating rate of 0.05 °C s<sup>-1</sup>. As the heating rate increases, the number density decreases while the precipitate size, on the contrary, increases. The average length and width of the precipitates have been determined on about 30 plates in the micrographs (an image processing routine would not give an accurate result). Results are presented in Table 4 in addition to the hardness measurements for each heating condition (30 kg load). The mean

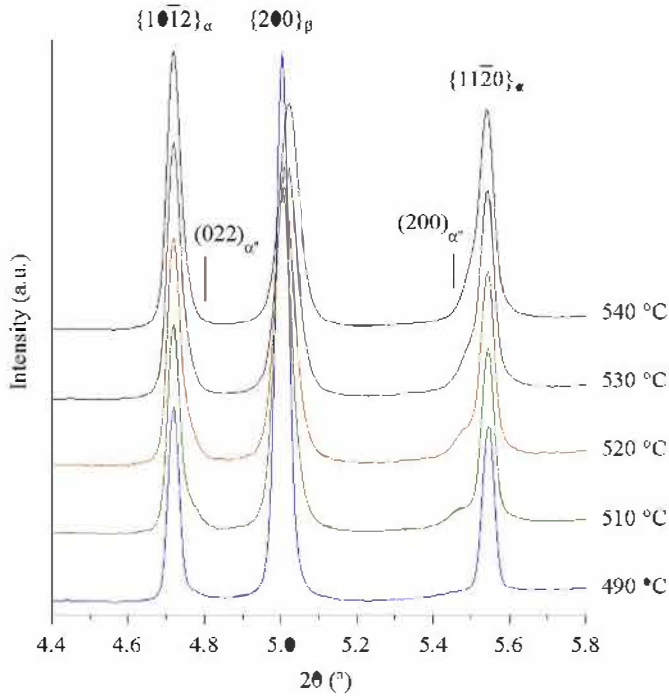


**Fig. 7.** Evolution of synchrotron X-ray diffraction patterns acquired during heating at the rate of  $0.1\text{ }^{\circ}\text{C s}^{-1}$ , after type “Colonies” initial heat treatment, between  $490\text{ }^{\circ}\text{C}$  and  $540\text{ }^{\circ}\text{C}$  where the formation of  $\alpha'$  isothermal metastable phase is evidenced.

width and length are doubled when the heating rate increases from  $0.1\text{ }^{\circ}\text{C s}^{-1}$  to  $1\text{ }^{\circ}\text{C s}^{-1}$ . It can be noticed though that the shape factor remains nearly constant for all heating rates. Moreover, the increasing number density of  $\alpha_{\text{secondary}}$  plates leads to an increase in the hardness values between the highest and lowest heating rates. Comparing rates of  $0.1\text{ }^{\circ}\text{C s}^{-1}$  and  $0.05\text{ }^{\circ}\text{C s}^{-1}$ , the sizes and densities of  $\alpha_{\text{secondary}}$  are more comparable, hence the similar hardness values for the two associate microstructures.

### 3.2. Influence of the initial microstructure

**Fig. 9** compares the evolution of the normed electrical resistivity during heating at a rate of  $1\text{ }^{\circ}\text{C s}^{-1}$ , for the three initial heat treatments, and during the one-hour isothermal holding at  $600\text{ }^{\circ}\text{C}$ . Following type “Colonies” and “Intragranular” initial heat treatments, the variations are very similar during almost the whole heating stage, with two changes of slope at  $210\text{ }^{\circ}\text{C}$  and  $320\text{ }^{\circ}\text{C}$  (**Fig. 9(a)**). However, the trends are different above  $480\text{ }^{\circ}\text{C}$ , where the electrical resistivity increases until  $600\text{ }^{\circ}\text{C}$  for type “Intragranular” initial heat treatment. This increase continues further for about 5 min during the isothermal holding before decreasing slightly and stabilizing at the end of the dwell (**Fig. 9(b)**). For type “Colonies” initial heat treatment, the electrical resistivity only starts to increase near  $600\text{ }^{\circ}\text{C}$  and during the dwell. When heating from an initial  $100\%\ \beta_{\text{metastable}}$  microstructure, the decrease in

electrical resistivity with temperature is much more significant and is observed until  $500\text{ }^{\circ}\text{C}$ . A slight increase in slope can also be noticed between  $220\text{ }^{\circ}\text{C}$  and  $330\text{ }^{\circ}\text{C}$ . Then, a sharp increase occurs between  $500\text{ }^{\circ}\text{C}$  and  $580\text{ }^{\circ}\text{C}$ . It is worth mentioning that for this type of initial heat treatment the electrical resistivity increases with the highest amplitude in this temperature domain. It then remains relatively constant during the isothermal holding at  $600\text{ }^{\circ}\text{C}$ .

The final bi-modal microstructure after ageing for the specimen submitted to type “Intragranular” initial heat treatment is shown in **Fig. 10(a)**. The amount (35%), morphology and distribution of  $\alpha_{\text{lam-prim}}$  are close to those before ageing. The volume fraction of  $\alpha_{\text{secondary}}$  plates is estimated at 26% as reported in **Table 5**. This value is of the same order of magnitude as for ageing treatments following type “Colonies” initial heat treatment. However, the average length and width of the plates are twice lower (**Table 6**) and the precipitate number density is much higher for this type “Intragranular” initial heat treatment.

Following type “100%  $\beta_{\text{m}}$ ” initial heat treatment, 62 vol.% of extremely thin  $\alpha$  precipitates have formed during ageing. Their thickness is about similar to the one of  $\alpha_{\text{secondary}}$  precipitates for type “Intragranular” initial heat treatment. However, there are important variations in length which can be associated with the size of the  $\beta$  matrix domains. The hardness value is the highest for this initial condition (most significant amount of thin  $\alpha_{\text{secondary}}$  precipitates). Comparing type “Colonies” and “Intragranular” initial heat treatments, a higher hardness is measured for the latter condition where the number density of refined  $\alpha_{\text{secondary}}$  plates is the highest.

## 4. Discussion

The results clearly reveal the influence of the heating conditions and the initial microstructure on the phase transformations sequences and kinetics in the  $\beta_{\text{metastable}}$  matrix during ageing, associated with the  $\alpha$  phase formation. This leads to significant differences in the final microstructures. However, one can emphasize first of all that the final  $\alpha$  phase volume fraction is close to 60% following all ageing conditions and for all initial microstructures considered. This one is below the fraction expected at equilibrium (77% by calculation at  $600\text{ }^{\circ}\text{C}$  on the Thermo-Calc<sup>®</sup> software using the TTTI3 titanium database).

### 4.1. Phase transformations when ageing an initial 100% $\beta_{\text{metastable}}$ microstructure

Amongst the studies of phase transformations on ageing in titanium alloys, some have reported the link between electrical resistivity variations and phase transformations when heating from initial  $100\%\ \beta_{\text{metastable}}$  initial microstructures [8–10] [12,34] [43–45], thanks to additional in-situ or post-mortem X-ray diffraction characterisations and also TEM observations. The evolutions of electrical resistivity observed for the  $100\%\ \beta_{\text{metastable}}$  initial microstructure in the present investigation are consistent with them.

Considering first of all the transformation kinetics when ageing

**Table 2**  
Crystallographic data of characteristic phases of Ti-based alloys used for HEXRD analysis.

Phase	Lattice system	Space group	Atomic positions	References
$\alpha$	Hexagonal	$P6_3/mmc$	$(1/3, 2/3, 1/4), (2/3, 1/3, 3/4)$	[42]
$\beta$	Cubic	$Im\bar{3}m$	$(0, 0, 0), (1/2, 1/2, 1/2)$	[42]
$\alpha'$	Orthorhombic	$Cmcm$	$(0, y, 1/4), (0, 1 - y, 3/4),$ $(1/2, 1/2 + y, 1/4), (1/2, 1/2 - y, 3/4)$	[36,40]
	Orthorhombic	$Fmmm$	Not given	[41]



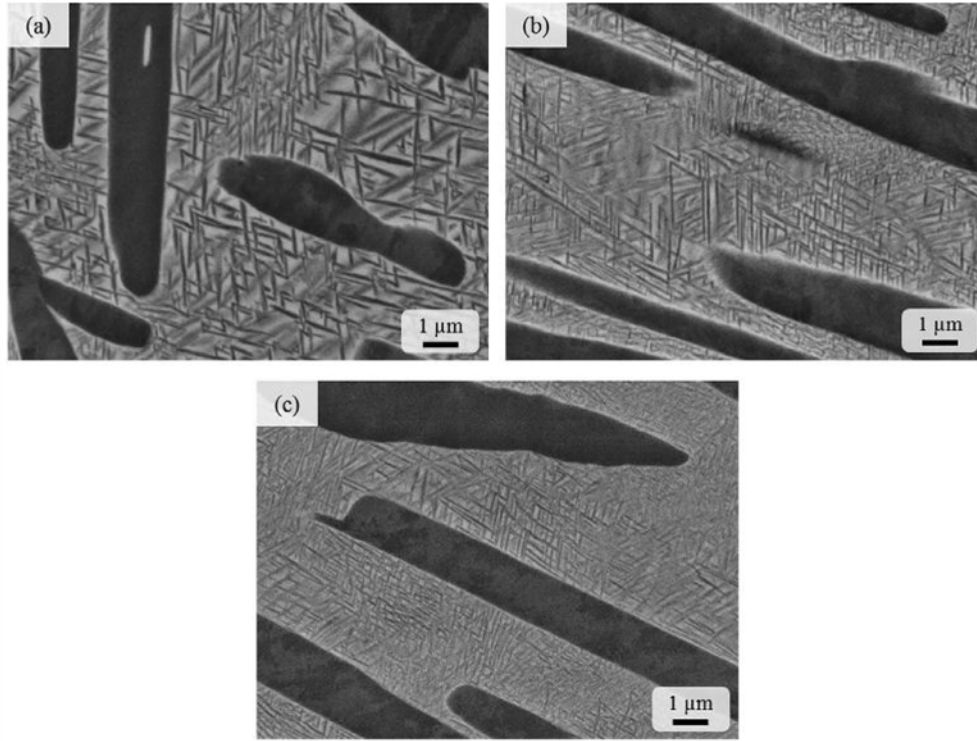


**Fig. 8.** SEM-BSE observation of the final microstructures of specimens aged at 600 °C with heating rates of (a) 1 °C s<sup>-1</sup>, (b) 0.1 °C s<sup>-1</sup> and (c) 0.05 °C s<sup>-1</sup> following type "Colonies" initial heat treatment.

**Table 3**

Volume fraction (%) of  $\alpha_{\text{lam-primary}}$  and  $\alpha_{\text{secondary}}$  as a function of the heating rate following ageing treatments for type "Colonies" initial heat treatment.

Heating rate	$\alpha_{\text{total}}$ fraction <sup>a</sup>	$\alpha_{\text{lam-primary}}$ fraction <sup>b</sup>	$\alpha_{\text{secondary}}$ fraction <sup>c</sup>
1 °C s <sup>-1</sup>	57 (±1)	35 (±1)	22
0.1 °C s <sup>-1</sup>	57 (±2)	34 (±1)	23
0.05 °C s <sup>-1</sup>	58 (±2)	35 (±1)	23

<sup>a</sup> Quantified by high energy X-ray diffraction.

<sup>b</sup> Quantified by image analysis.

<sup>c</sup> Difference in the  $\alpha_{\text{total}}$  fraction and the  $\alpha_{\text{lam-primary}}$  fraction.

**Table 4**

Average  $\alpha_{\text{secondary}}$  size and Vickers hardness measurements as a function of the heating rate following ageing treatments.

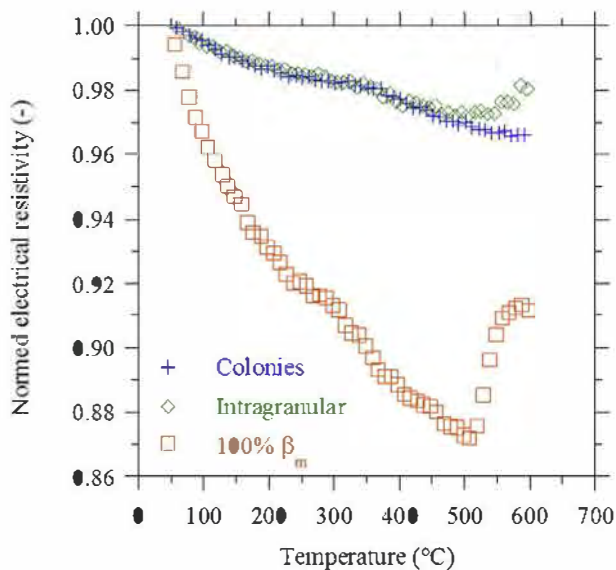
Heating rate	Length (μm)	Width (μm)	HV30
1 °C s <sup>-1</sup>	1.10 (±0.26)	0.120 (±0.02)	386 (±2)
0.1 °C s <sup>-1</sup>	0.51 (±0.08)	0.064 (±0.01)	401 (±4)
0.05 °C s <sup>-1</sup>	0.41 (±0.20)	0.051 (±0.01)	402 (±2)

the 100%  $\beta_{\text{metastable}}$  state, the evolution of the electrical resistivity during heating at a rate of 1 °C s<sup>-1</sup> (Fig. 9(a)) suggests that phase transformations occur in two temperature domains: 220 °C - 330 °C and 500 °C - 580 °C. These evolutions are also marked by a sharp initial decrease when heating begins from room temperature. This is referred to as the "Negative Temperature Dependence" (NTD) effect. It is associated with the presence of the  $\omega_{\text{athermal}}$  phase (hexagonal structure) in the  $\beta_{\text{metastable}}$  phase [44,46], which precipitated at low temperature during quenching from above the  $\beta$  transus temperature. This metastable phase is very difficult to be detected by high energy X-ray diffraction, but is clearly revealed by electron diffraction in a TEM [10,33,35,45,47].

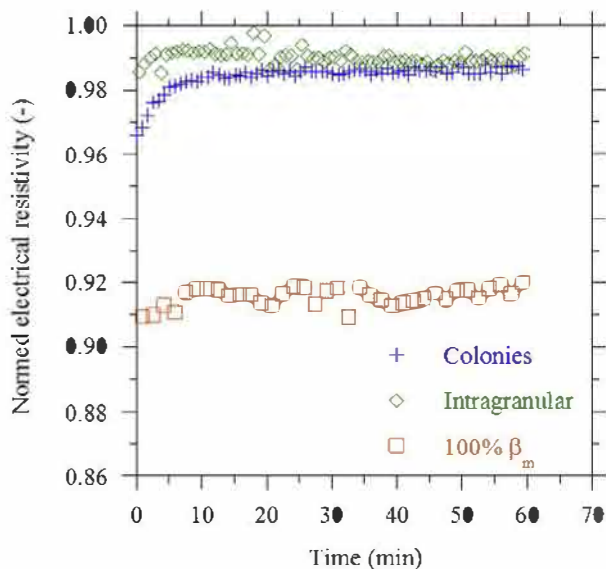
In the temperature domain 220 °C–330 °C, several studies on near- $\beta$  using X-ray diffraction (Ti-12Mo [45]) or electron diffraction

(Ti-5553 [33],  $\beta\text{Cez}$  [9], Ti-LCB [48] or Ti-6Mo-5Ta-4Fe [34]) enable to associate the change of slope in electrical resistivity to the precipitation of  $\omega_{\text{isothermal}}$  phase. The nucleation of this metastable phase is considered favoured by the remaining  $\omega_{\text{athermal}}$  [33,49]. For temperatures above 330 °C, a change in slope is again observed in the electrical resistivity variations. This one is relatively slight as compared to the positive slopes reported by Bruneseaux et al. for Ti-17 alloy at a heating rate of 0.7 °C s<sup>-1</sup> [50], Settefrati et al. for Ti-5553 alloy [12] and Chang et al. for Ti-B19 alloy [15] at a rate of 0.1 °C s<sup>-1</sup>. In their investigations, in-situ HEXRD experiments allowed to link the change of slope in electrical resistivity to further precipitation of the  $\omega_{\text{isothermal}}$  phase, as well as to the formation of an orthorhombic phase (called  $\alpha''_{\text{isothermal}}$ ). This latter phase has been observed by HEXRD to form either during isothermal ageing after a relatively long annealing time [51] or during continuous heating at rates no higher than 0.5 °C s<sup>-1</sup> [11,12,14,15]. It was considered as a base centered orthorhombic structure like the martensite structure obtained upon quenching. From TEM studies, the precipitation of an additional phase characterized as the  $\alpha$  phase with an hexagonal structure was reported [35,48]. However, based on a recent TEM analysis, the formation of an orthorhombic face centered structure ( $O''$ ) is proposed [41]. This structure is generally reported to nucleate from/in the vicinity of  $\omega_{\text{isothermal}}$  precipitates [14,33,35,37,48].

A progressive decrease in intensity and vanishing of the  $\omega$  peaks was also observed during these in-situ HEXRD experiments, while those of  $\alpha''_{\text{isothermal}}$  increased in intensity. More precisely, this  $\omega_{\text{isothermal}}$  phase has been widely considered to act as heterogeneous nucleation sites for the  $\alpha$  phase [14,33,35,48,52,53], in the case of slow heating conditions, arising from additional driving forces through compositional and/or stress variations associated with the  $\omega_{\text{isothermal}}$  phase evolution [33,54]. As temperature increases and gets closer to 600 °C, past studies on Ti-5553 [18] and Ti-5553-1Zr [14] alloys reported that the  $\alpha''_{\text{isothermal}}$  orthorhombic



(a)



(b)

**Fig. 9.** Evolution of the normed electrical resistivity during ageing at 600 °C following each type of initial heat treatment: (a) heating at a rate of 1 °C s<sup>-1</sup> and (b) one-hour isothermal holding.

structure evolves and tends towards the hexagonal close packed  $\alpha$  structure. This evolution has also been observed during ageing of the orthorhombic  $\alpha''$  martensite formed upon quenching in Ti-10V-2Fe-3Al [37,55] and Ti-6Al-6V-2Sn [56] alloys. In consequence to that global precipitation sequence, the final microstructure generally consisted in a very high density of small  $\alpha$  precipitates of which the aspect ratio (width/length) strongly increases [12,33].

The heating condition considered in the present investigation (1 °C s<sup>-1</sup>) led to a decrease in electrical resistivity above 330 °C which is thus associated with a low amount of  $\alpha''$  isothermal that nucleated from  $\omega$  isothermal precipitates. The significant increase when reaching temperatures of 500 °C–600 °C indicates the further nucleation and growth of  $\alpha''$  isothermal precipitates which evolve towards the  $\alpha$  phase structure. The final microstructure (Fig. 10(b)) shows  $\alpha$  lamellae with a lower aspect ratio. This change

in morphology can be associated with the lower amount of  $\omega$  isothermal precipitates formed, and in consequence to a lower nucleation rate for  $\alpha''$  isothermal/ $\alpha$ . The existing nuclei will thus grow more and adopt a lamellar morphology that minimizes the elastic stored energy [57,58].

#### 4.2. Ageing of initial $\alpha_{lam\text{-}primary} + \beta_{metastable}$ microstructures

##### 4.2.1. Influence of the $\alpha_{lam\text{-}primary}$ morphology

Ageing treatment of types “Colonies” and “Intragranular” mainly leads to the partial transformation of the remaining metastable  $\beta$  phase (about 70 vol.%), as no significant evolution in the fraction or morphology of the  $\alpha_{lam\text{-}primary}$  lamellae has been observed for all considered heat treatment conditions. Due to the initial presence of  $\alpha$  phase, the behavior on heating differs from that of 100%  $\beta_{metastable}$  and affects the electrical resistivity. On the one hand, the difference in the mean slope during heating can be associated with the initial ( $\alpha + \beta$ ) mixture. On the other hand, there are also changes of slope associated to the precipitation of metastable phases in different temperature domains.

**4.2.1.1. Phase transformation kinetics.** The first significant difference is the initial mean slope when heating between room temperature and 200 °C, also negative but at a much less extent as compared to the initial 100%  $\beta_{metastable}$  microstructure (Fig. 9(a)). Qualitatively, this slope is even less negative compared to an initial 15%  $\alpha_{primary}$  microstructure in Ti-5553 alloy [12]. It thus appears the influence of the initial  $\alpha$  phase amount on the NTD effect, even if  $\omega$  athermal precipitates have been observed in the initial microstructures (Fig. 4). Indeed, electrical resistivity variations of a ( $\alpha + \beta$ ) mixture with a high amount of  $\alpha$  phase show a positive slope as temperature increases. Such a slope is typically obtained below 400 °C when performing continuous cooling heat treatments [59]. Moreover, as a result of the holding at 800 °C for types “Colonies” and “Intragranular” initial heat treatments ( $\approx 35$  vol.% initial  $\alpha_{lam\text{-}primary}$ ), it can be assumed that the  $\beta_{metastable}$  phase is enriched in  $\beta$ -stabilizing elements following quenching. This possibly led to a higher density and/or coarser size distribution of  $\omega$  athermal precipitates in the remaining  $\beta$  phase, making their observation in dark field mode easier. These two contributions can consequently affect the initial mean slope.

Secondly, a first change of slope is observed in the temperature range 210 °C–320 °C for both initial ( $\alpha_{lam\text{-}primary} + \beta_{metastable}$ ) microstructures. These are approximately identical between them and are associated with the formation of  $\omega$  isothermal as described previously. However, due to the low deviations, the amount of precipitates formed can be expected low. As temperature increases, the increase in electrical resistivity at 480 °C for the initial “Intragranular” microstructure indicates the beginning of  $\alpha''$  isothermal/ $\alpha$  phase precipitation. The precipitation then progresses during the further heating and holding stage. For the initial “Colonies” microstructure, on the contrary, precipitation only begins during the holding stage at 600 °C (Fig. 9). The kinetics are thus slower for the initial ( $\alpha_{lam\text{-}primary} + \beta_{metastable}$ ) initial microstructure as compared to the fully metastable initial state, considering on the one hand the important increase in electrical resistivity (slope and amplitude of the curve), and on the other hand the more restricted temperature domain (entirely during heating).

Even though different precipitation kinetics between the “100%  $\beta_m$ ” and the ( $\alpha_{lam\text{-}primary} + \beta_{metastable}$ ) initial microstructures could be anticipated, it was less obvious between the “Colonies” and “Intragranular” ones. Such differences could arise from the chemical driving force linked to the chemical composition of the  $\beta_{metastable}$  phase. However, this chemical composition can be considered similar for these two ( $\alpha_{lam\text{-}primary} + \beta_{metastable}$ ) initial

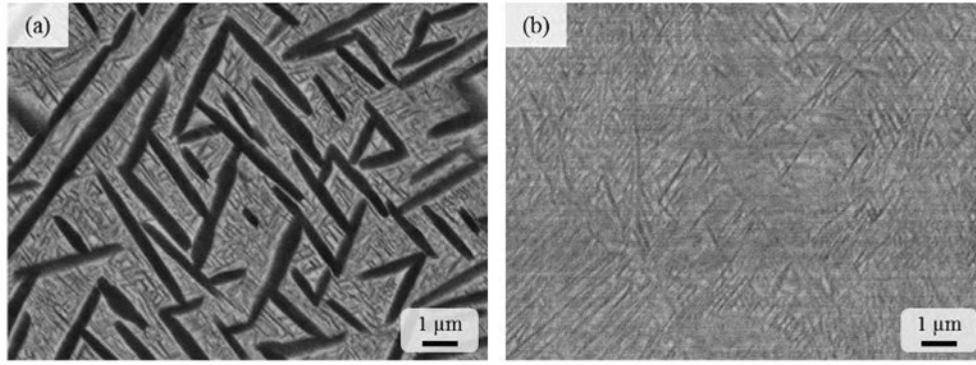


**Fig. 10.** Final microstructure after ageing at a rate of  $1\text{ }^{\circ}\text{C s}^{-1}$  following (a) type "Intragranular" and (b) type "100%  $\beta_m$ " initial heat treatment.

**Table 5**

Volume fraction (%) of  $\alpha_{\text{lam-primary}}$  and  $\alpha_{\text{secondary}}$  as a function of the initial microstructure following ageing treatments (heating rate:  $1\text{ }^{\circ}\text{C s}^{-1}$ ).

Initial heat treatment	$\alpha_{\text{total}}$ fraction <sup>a</sup>	$\alpha_{\text{lam-primary}}$ fraction <sup>b</sup>	$\alpha_{\text{secondary}}$ fraction <sup>c</sup>
Colonies	57 ( $\pm 1$ )	35 ( $\pm 1$ )	22
Intragranular	61 ( $\pm 1$ )	35 ( $\pm 1$ )	26
100% $\beta_m$	62 ( $\pm 1$ )	0	62

<sup>a</sup> Quantified by high energy X-ray diffraction.

<sup>b</sup> Quantified by image analysis.

<sup>c</sup> Difference in the  $\alpha_{\text{total}}$  fraction and the  $\alpha_{\text{lam-primary}}$  fraction.

**Table 6**

Average  $\alpha_{\text{secondary}}$  size and Vickers hardness measurements as a function of the initial microstructure following ageing treatments (heating rate:  $1\text{ }^{\circ}\text{C s}^{-1}$ ).

Initial heat treatment	Length ( $\mu\text{m}$ )	Width ( $\mu\text{m}$ )	HV30
Colonies	1.10 ( $\pm 0.26$ )	0.120 ( $\pm 0.02$ )	386 ( $\pm 2$ )
Intragranular	0.44 ( $\pm 0.1$ )	0.051 ( $\pm 0.01$ )	410 ( $\pm 2$ )
100% $\beta_m$	/	/	459 ( $\pm 4$ )

microstructures since similar  $\alpha_{\text{lam-primary}}$  volume fractions were quantified. Consequently, the chemical driving force is considered the same. Additional features thus need to be considered. It can be mentioned that the spatial distribution of  $\alpha_{\text{lam-primary}}$  precipitates in the "Intragranular" microstructure results in shorter inter-lamellar gaps and restricted  $\beta$  domains. This geometrical pattern may generate different strain fields during quenching when forming the initial microstructure, or influence the elastic interaction energy during the transformation during ageing. These features have to be taken into account and further analyzed.

**4.2.1.2. Final  $\alpha_{\text{secondary}}$  precipitation state.** The evolutions of electrical resistivity evidence that the transformation of the  $\beta_{\text{metastable}}$  phase occurs mainly at high temperature (above  $500\text{ }^{\circ}\text{C}$ ) with the nucleation and growth of  $\alpha''_{\text{isothermal}}/\alpha$  as temperature increases. Thin lamellae are systematically formed, but of which the density decreases and the width increases as the transformation temperature domain increases. This can be clearly observed in Figs. 8(a) and 10(a) and (b) for the "Colonies", "Intragranular" and "100%  $\beta_m$ " initial microstructures respectively. The higher number density of  $\alpha_{\text{secondary}}$  plates is associated with  $\alpha''_{\text{isothermal}}/\alpha$  nucleation that begins at a lower temperature. Consequently, the higher number of nuclei involved limits the growth of the lamellae. If nucleation begins at a higher temperature, the available driving force is lower and the nucleation kinetics slower. The number of nuclei involved is reduced and those formed are able to grow at a larger extent. The final microstructures thus exhibit a much finer distribution of  $\alpha_{\text{secondary}}$  plates for the initial "100%  $\beta_m$ " and "Intragranular"

microstructures. On the contrary, the plates are coarser and with a lower number density in the "Colonies" initial microstructure. The higher hardness values measured for the first two initial microstructures (Table 6) confirm the microstructural strengthening mainly brought by the extreme thin size and high number density of the  $\alpha_{\text{secondary}}$  plates.

#### 4.2.2. Influence of the heating rate on precipitation kinetics

Complementary to the study of the influence of the initial microstructure, the influence of the ageing conditions for a same initial microstructure, but consisting of  $\approx 35\%$   $\alpha_{\text{lam-primary}}$  (type "Colonies" initial heat treatment), was investigated. This involved heating at rates of  $0.05\text{ }^{\circ}\text{C s}^{-1}$  (slow heating rate) and  $0.1\text{ }^{\circ}\text{C s}^{-1}$  (intermediate heating rate), in addition to  $1\text{ }^{\circ}\text{C s}^{-1}$ . The variations of electrical resistivity for these three rates (Fig. 5(a)) clearly suggest that phase transformations occur in similar temperature ranges as for the two other initial microstructures heated at  $1\text{ }^{\circ}\text{C s}^{-1}$ :  $200\text{ }^{\circ}\text{C}$  -  $300\text{ }^{\circ}\text{C}$  and  $450\text{ }^{\circ}\text{C}$  -  $600\text{ }^{\circ}\text{C}$ . However, the kinetics vary with the heating rate.

**4.2.2.1. Formation of  $\omega_{\text{isothermal}}$ .** In the first temperature range, the kinetics of  $\omega_{\text{isothermal}}$  precipitation are similar for all three conditions. However, when heating is performed at  $0.05\text{ }^{\circ}\text{C s}^{-1}$ , the significant electrical resistivity increase indicates a higher amount of  $\omega_{\text{isothermal}}$ . For the intermediate and fast heating rates, some precipitation can be expected considering the slight changes of slope with temperature. Nevertheless, the amount must be much reduced as the heating rate increases. Moreover, HEXRD experiments carried out at the rate of  $0.1\text{ }^{\circ}\text{C s}^{-1}$  did not allow to evidence any  $\omega$  peaks (Fig. 6).

**4.2.2.2. Formation of  $\alpha''_{\text{isothermal}}/\alpha$ .** The further increase in electrical resistivity between  $460\text{ }^{\circ}\text{C}$  and  $580\text{ }^{\circ}\text{C}$  for heating rates of  $0.05\text{ }^{\circ}\text{C s}^{-1}$  and  $0.1\text{ }^{\circ}\text{C s}^{-1}$  is clearly associated with the precipitation of  $\alpha''_{\text{isothermal}}/\alpha$ . Indeed, the in-situ HEXRD characterisations for the intermediate heating rate revealed the orthorhombic character of the structure, observed on diffraction patterns between  $490\text{ }^{\circ}\text{C}$  and  $540\text{ }^{\circ}\text{C}$  as shoulders near  $\{10\bar{1}2\}_{\alpha}$  and  $\{11\bar{2}0\}_{\alpha}$  peaks (Fig. 7). These shoulders could be indexed as  $(022)$  and  $(200)$   $\alpha''_{\text{isothermal}}$  peaks and were also reported in Ti-5553 for a similar heating rate ( $0.14\text{ }^{\circ}\text{C s}^{-1}$ ) and an initial ( $15\%$   $\alpha_{\text{primary}}$  +  $\beta_{\text{metastable}}$ ) microstructure [12]. Their intensity then gradually diminished while the intensity of the  $\alpha$  peaks increased with temperature. HEXRD thus confirms the link between the increase in electrical resistivity and the precipitation of  $\alpha''_{\text{isothermal}}/\alpha$ . For the fast heating rate,  $\alpha''_{\text{isothermal}}$  precipitation is much more restricted as electrical resistivity only increases from about  $600\text{ }^{\circ}\text{C}$ , indicating slower kinetics.

A quantitative characterisation of the diffraction patterns led to

the evolution of the volume fractions and the mean cell parameters of the  $\alpha''$ ,  $\alpha$  and  $\beta$  phases, as a function of temperature, for the heating rate of  $0.1\text{ }^\circ\text{C s}^{-1}$ . These are reported in Fig. 11. Results confirm an increase in the  $(\alpha''_{\text{isothermal}} + \alpha)$  phase volume fraction between  $500\text{ }^\circ\text{C}$  and  $560\text{ }^\circ\text{C}$ , while that of the  $\beta$  phase decreases, before stabilization up to  $600\text{ }^\circ\text{C}$ . The analysis of the lattice parameters evolution reveals an associate decrease of  $a_\beta$ , mainly consistent with a change in the chemical composition of the parent phase due to the partitioning of solute elements as the transformation progresses (notably the enrichment of  $\beta$ -stabilizing elements). This points out the diffusive character for the formation of the  $\alpha''_{\text{isothermal}}$  precipitates. Their mean cell parameters vary progressively and evolve towards those of  $\alpha$ . This tendency is marked by a sharp decrease of  $a_{\alpha''}$  and an increase of  $c_{\alpha''}$  between  $500\text{ }^\circ\text{C}$  and  $560\text{ }^\circ\text{C}$ , before more moderate evolutions up to the ageing temperature (the  $\alpha$  phase is considered as an orthorhombic structure with  $b_\alpha = a_\alpha \cdot \sqrt{3}$ ). These variations can be associated with a change in the chemical composition of the  $\alpha''_{\text{isothermal}}$  phase. The chemical composition of the precipitates formed at the lower temperatures is thus far from the equilibrium composition. As temperature increases and diffusion is more effective, their chemical composition tends towards the equilibrium one.

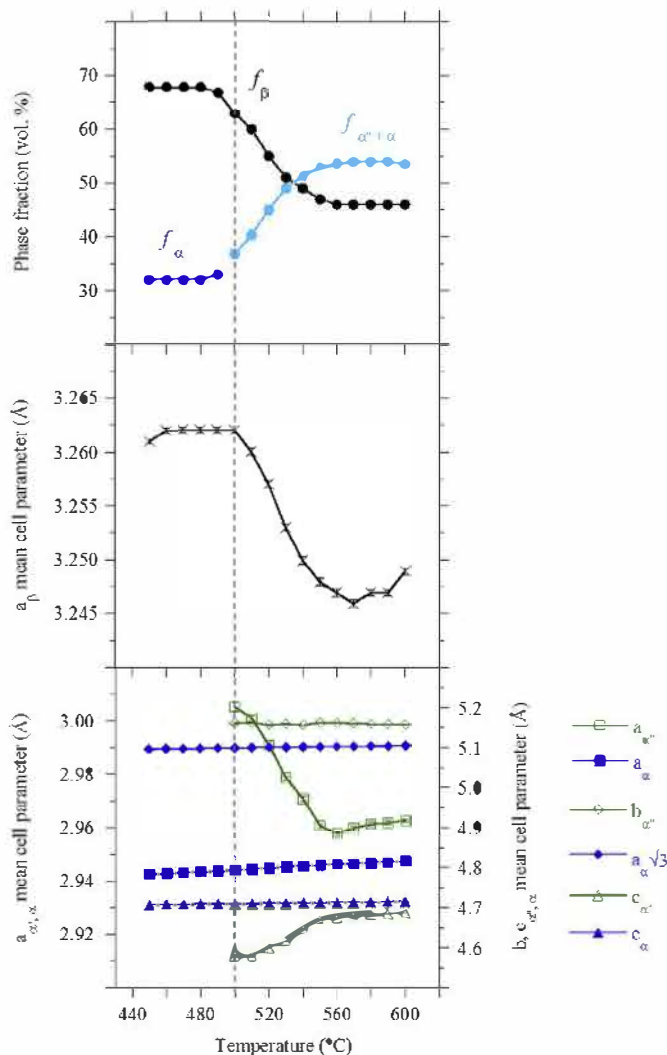


**Fig. 11.** Evolution of the volume fractions and mean cell parameters of the  $\alpha''_{\text{isothermal}}$ ,  $\alpha$  and  $\beta$  phases during heating at the rate of  $0.1\text{ }^\circ\text{C s}^{-1}$  determined by in-situ HEXRD. The refinement uncertainty is comprised within the symbols.

The orthorhombic structure of the  $\alpha''_{\text{isothermal}}$  phase originates from stress and strain fields arising from the  $\beta \rightarrow \alpha$  transformation [60,61], and also the chemical compositions of the precipitates formed which differ from that of the equilibrium  $\alpha$  phase in early precipitation stages, as reported in previous investigations on analogous Ti-5553 [35,62] or Ti-LCB [8] alloys. The evolutions of the mean cell parameters, together with the evolution of the  $\alpha''_{\text{isothermal}}$  and  $\alpha$  peaks described previously, suggest that there is indeed a gradual evolution of the orthorhombic structure towards the hexagonal close-packed structure.

Finally, it can also be mentioned that this in-situ characterisation led to a total  $(\alpha''_{\text{isothermal}} + \alpha)$  phase volume fraction of 53% at  $600\text{ }^\circ\text{C}$  (without isothermal holding). The post-mortem characterisation presented in Table 3 for the same heating rate but with an additional isothermal holding of 1 h at  $600\text{ }^\circ\text{C}$  gave a total  $\alpha$  fraction of 57 vol.%. There is thus further precipitation during the dwell but such a holding is not long enough to reach a calculated equilibrium fraction as mentioned previously.

**4.2.2.3. Final aged microstructures.** The observation of the resulting microstructures (Fig. 8), and associate quantitative characterisations (Table 4), showed significant variations in terms of morphology, size and precipitation number density of  $\alpha_{\text{secondary}}$  plates that are the consequence of the phase transformations highlighted by in-situ electrical resistivity measurements and HEXRD. Coarser plates were obtained when heating at  $1\text{ }^\circ\text{C s}^{-1}$  for which the amount of  $\omega$  phase formed is reduced and the kinetics of subsequent nucleation of  $\alpha''_{\text{isothermal}}/\alpha$  are slower. As the heating rate decreased, nucleation of  $\alpha''_{\text{isothermal}}$  occurred at lower temperatures with a higher nucleation rate, leading on the contrary to a fine and dense distribution of  $\alpha_{\text{secondary}}$  plates. This microstructural refinement, obtained in this study for an initial  $\approx 35\%$   $\alpha_{\text{lam-primary}}$ , is consistent with the previous investigations on a  $100\%$   $\beta_{\text{metastable}}$  state in Ti-5553 [12,33] or Ti-5553-1Zr [14] alloys. Consequently, the hardness increases but a lower elongation at failure could be expected for these microstructural features [17,63].

## 5. Conclusion

In this contribution, the use of in-situ electrical resistivity combined with high energy X-ray diffraction enabled to study the precipitation sequences and kinetics during ageing treatment in Ti-17 alloy, with an initial microstructure  $100\%$   $\beta_{\text{metastable}}$  or consisting of about  $35\%$   $\alpha + 65\%$   $\beta_{\text{metastable}}$  (vol.%). The following conclusions can be drawn:

- (1) For these three initial microstructures, the same phase transformations may successively occur during ageing, i.e. formation of  $\omega_{\text{isothermal}}$  and of  $\alpha''_{\text{isothermal}}/\alpha$ .
- (2) The influence of the heating rate on the final microstructure of  $\alpha_{\text{secondary}}$  is confirmed for an initial  $35\%$   $\alpha_{\text{lam-primary}} + \beta_{\text{metastable}}$  microstructure. The size and number density of these precipitates strongly depend on the precipitation sequences and their kinetics, which vary with the heating rate during ageing treatments:
  - The transformation path  $\alpha''_{\text{isothermal}} \rightarrow \alpha$  is confirmed by in-situ high-energy X-ray diffraction for a low heating rate in the temperature range  $500\text{ }^\circ\text{C} - 560\text{ }^\circ\text{C}$ .
  - The precipitation of a refined and homogeneous distribution of  $\alpha$  plates observed for low heating rates ( $0.05\text{ }^\circ\text{C s}^{-1}$  and  $0.1\text{ }^\circ\text{C s}^{-1}$ ) is associated with the precipitation of  $\omega_{\text{isothermal}}$  phase as well as a significant and rapid nucleation of  $\alpha''_{\text{isothermal}}/\alpha$  beginning at lower temperatures. For higher heating rates, the reduced amount of  $\omega_{\text{isothermal}}$  phase formed leads mainly to the nucleation of  $\alpha''_{\text{isothermal}}/\alpha$  at

higher temperatures with a lower nucleation rate, resulting in coarser precipitates with a lower precipitation number density.

- (3) The initial ( $\alpha_{\text{lam-primary}} + \beta_{\text{metastable}}$ ) microstructure influences notably the  $\alpha''_{\text{isothermal}}/\alpha$  precipitation kinetics during ageing as compared to an initial 100%  $\beta_{\text{metastable}}$  microstructure for the considered heating rate (1 °C/s):
- An initial “Colonies” microstructure shifts the  $\alpha''_{\text{isothermal}}/\alpha$  transformation temperature range to higher temperatures, resulting in coarser  $\alpha_{\text{secondary}}$  plates. On the contrary, an initial “Intragranular” microstructure leads to a fine and dense distribution of  $\alpha_{\text{secondary}}$  plates formed at lower temperatures with quicker kinetics.
  - For a similar  $\alpha_{\text{lam-primary}}$  fraction, the different precipitation kinetics of  $\alpha_{\text{secondary}}$  highlight the probable influence of stress and strain states linked to the spatial distribution, size and inter-lamellar gap between initial  $\alpha_{\text{lam-primary}}$  precipitates.

## Acknowledgements

This work was supported by the French National Research Agency under the framework of the ANR-DUSTI project (grant number ANR-13-RMNP-0014), as well as the Labex DAMAS of the Université de Lorraine. The authors also thank the European Synchrotron Radiation Facility (ESRF) and the Deutsches Elektronen Synchrotron (DESY) for providing beamline time, Dr. Guillaume Geandier (Institut Jean Lamour) for help provided during the experiments and all the partners of the ANR-DUSTI project for fruitful discussions.

## References

- [1] S. Audion, G. Khelifati, J. Delfosse, P.-Y. Ouilic, R. Peraldi, Extending the use of titanium alloys on A350XWB, in: Proceedings of the 12th World Conference on Titanium, 2012.
- [2] M. Peters, J. Kumpfert, C.H. Ward, C. Leyens, Titanium alloys for aerospace applications, *Adv. Eng. Mater.* 5 (6) (2003) 419–427.
- [3] R.R. Boyer, An overview on the use of titanium in the aerospace industry, *Mater. Sci. Eng. A* 213 (1–2) (1996) 103–114.
- [4] R.R. Boyer, R.D. Briggs, The use of  $\beta$  titanium alloys in the aerospace industry, *J. Mater. Eng. Perform.* 14 (6) (2005) 681–685.
- [5] O.M. Ivasishin, P.E. Markovsky, Y.V. Matviychuk, S.L. Semiatin, C.H. Ward, S. Fox, A comparative study of the mechanical properties of high-strength  $\beta$ -titanium alloys, *J. Alloys. Compd.* 457 (1–2) (2008) 296–309.
- [6] F. Bruneseaux, et al., In situ characterizations of phase transformations kinetics in the Ti17 titanium alloy by electrical resistivity and high temperature synchrotron X-ray diffraction, *Mater. Sci. Eng. A* 476 (1–2) (2008) 60–68.
- [7] M. Salib, J. Teixeira, L. Germain, E. Lamielle, N. Gey, E. Aeby-Gautier, Influence of transformation temperature on microtexture formation associated with  $\alpha$  precipitation at  $\beta$  grain boundaries in a  $\beta$  metastable titanium alloy, *Acta Mater.* 61 (10) (2013) 3758–3768.
- [8] O.M. Ivasishin, P.E. Markovsky, S.L. Semiatin, C.H. Ward, Aging response of coarse- and fine-grained  $\beta$  titanium alloys, *Mater. Sci. Eng. A* 405 (1–2) (2005) 296–305.
- [9] R. Sanguinetti, M. Zandona, A. Pianelli, E. Gautier, Decomposition of  $\beta$ -metastable Phase in  $\beta$ -CeZ alloy during continuous heating, *J. Phys. IV* 3 (C7) (1993) 527–531.
- [10] F. Prima, P. Vermaut, D. Ansel, J. Debuigne,  $\omega$  precipitation in a beta metastable titanium alloy, resistometric study, *Mater. Trans., JIM* 41 (8) (2000) 1092–1097.
- [11] F. Bruneseaux, G. Geandier, E. Gautier, M. Dehmas, P. Boulet, In situ characterization of the transformation sequences of Ti17 alloy by high energy X-ray Diffraction. Influence of the thermal path, in: Proceedings of the 11th World Conference on Titanium, 2007.
- [12] A. Settefrati, et al., Precipitation in a near beta titanium alloy on ageing: influence of heating rate and chemical composition of the beta-metastable phase, *Sol-Sol Ph. Transform. Inorg. Mater.* 172–174 (2011) 760–765.
- [13] N.G. Jones, R.J. Dashwood, M. Jackson, D. Dye,  $\beta$  Phase decomposition in Ti–5Al–5Mo–5V–3Cr, *Acta Mater.* 57 (13) (2009) 3830–3839.
- [14] P. Barriobero-Vila, G. Requena, S. Schwarz, F. Warchomicka, T. Buslaps, Influence of phase transformation kinetics on the formation of  $\alpha$  in a  $\beta$ -quenched Ti–5Al–5Mo–5V–3Cr–1Zr alloy, *Acta Mater.* 95 (2015) 90–101.
- [15] H. Chang, E.A. Gautier, L. Zhou, Phase transformation kinetics in metastable titanium alloys, *Chin. Sci. Bull.* 59 (15) (2014) 1773–1777.
- [16] M. Bönisch, et al., Giant thermal expansion and  $\alpha$ -precipitation pathways in Ti-alloys, *Nat. Commun.* 8 (2017) 1429.
- [17] E. Aeby-Gautier, B. Denand, J. Teixeira, M. Dehmas, B. Appolaire, A. Settefrati, Influence of microstructure on tensile properties of  $\beta$ -metastable Ti 17 alloy, in: Proceedings of the 12th World Conference on Titanium, vol. 2, 2011, pp. 1191–1195.
- [18] A. Settefrati, Étude expérimentale et modélisation par champ de phase de la formation de  $\alpha$  dans les alliages de titane  $\beta$ -métastable, Thèse de doctorat, Université de Lorraine, 2012.
- [19] T. Duval, Analyse multi-échelles des relations microstructure/propriétés mécaniques sous sollicitation monotone et cyclique des alliages de titane  $\beta$ -métastable, Thèse de doctorat, Ecole Nationale Supérieure de Mécanique et d'Aérotechnique, 2013.
- [20] T. Duval, P. Villechaise, S. Andrieu, Mechanical properties and strain mechanisms analysis in Ti-5553 titanium alloys, *TMS2011 Suppl. Proc.* 3 (2011) 471–478.
- [21] E. Lebrun, P. Svec, Y. Millet, S. Andrieu, F. Prima, Investigation of  $\alpha$  phase precipitation mode during ageing treatment in Ti-18 alloy, in: Proceedings of the 13th World Conference on Titanium, 2016.
- [22] E. Laude, E. Gautier, P. Archambault, S. Denis, Effects of thermomechanical treatments on the transformation kinetics of titanium alloys. Experimental study and numerical calculation, *Rev. De Metall. CIT/Sci. Et Génie des Matér.* 93 (9) (1996) 1067–1078.
- [23] P. Archambault, D. Godard, High temperature precipitation kinetics and TTT curve of a 7xxx alloy by in-situ electrical resistivity measurements and differential calorimetry, *Scripta Mater.* 42 (7) (2000) 675–680.
- [24] G. Geandier, E. Aeby-Gautier, A. Settefrati, M. Dehmas, B. Appolaire, Study of diffusive transformations by high energy X-ray diffraction, *Compt. Rendus Phys.* 13 (3) (2012) 257–267.
- [25] H.M. Rietveld, A profile refinement method for nuclear and magnetic structures, *J. Appl. Crystallogr.* 2 (2) (1969) 65–71.
- [26] J. Rodríguez-Carvajal, Recent advances in magnetic structure determination by neutron powder diffraction, *Phys. B Condens. Matter* 192 (1–2) (1993) 55–69.
- [27] A.P. Hammersley, S.O. Svensson, A. Thompson, Calibration and correction of spatial distortions in 2D detector systems, *Nucl. Instrum. Methods Phys. Res. Sect. A Accel. Spectrom. Detect. Assoc. Equip.* 346 (1) (1994) 312–321.
- [28] M. Coster, J.-L. Chermant, Précis D'analyse D'images, 1985.
- [29] “ADCIS Products: AphelionTM Dev.” [Online]. Available: <http://www.adcis.net/en/Products/Aphelion-Dev-4.x/Overview.html>.
- [30] J.D.C. Teixeira, B. Appolaire, E. Aeby-Gautier, S. Denis, G. Cailletaud, N. Späth, Transformation kinetics and microstructures of Ti17 titanium alloy during continuous cooling, *Mater. Sci. Eng. A* 448 (1–2) (2007) 135–145.
- [31] H. Sharma, S.M.C. van Bohemen, R.H. Petrov, J. Sietsma, Three-dimensional analysis of microstructures in titanium, *Acta Mater.* 58 (7) (2010) 2399–2407.
- [32] Thermodynamic databases - Thermo-Calc Software.” [Online]. Available: <http://www.thermocalc.com/products-services/databases/thermodynamic/>.
- [33] Y. Zheng, et al., Role of  $\omega$  phase in the formation of extremely refined intragranular  $\alpha$  precipitates in metastable  $\beta$ -titanium alloys, *Acta Mater.* 103 (2016) 850–858.
- [34] T. Gloriant, G. Texier, F. Sun, I. Thibon, F. Prima, J.L. Soubeyroux, Characterization of nanophase precipitation in a metastable  $\beta$  titanium-based alloy by electrical resistivity, dilatometry and neutron diffraction, *Scripta Mater.* 58 (4) (2008) 271–274.
- [35] S. Nag, R. Banerjee, R. Srinivasan, J.Y. Hwang, M. Harper, H.L. Fraser,  $\omega$ -Assisted nucleation and growth of  $\alpha$  precipitates in the Ti–5Al–5Mo–5V–3Cr–0.5Fe  $\beta$  titanium alloy, *Acta Mater.* 57 (7) (2009) 2136–2147.
- [36] A.R.G. Brown, D. Clark, J. Eastbrook, K.S. Jepson, The titanium–niobium system, *Nature* 201 (4922) (1964) 914–915.
- [37] P. Barriobero-Vila, G. Requena, F. Warchomicka, A. Stark, N. Schell, T. Buslaps, Phase transformation kinetics during continuous heating of a  $\beta$ -quenched Ti–10V–2Fe–3Al alloy, *J. Mater. Sci.* 50 (3) (2015) 1412–1426.
- [38] E.G. Obbard, et al., The effect of oxygen on  $\alpha'$  martensite and superelasticity in Ti–24Nb–4Zr–8Sn, *Acta Mater.* 59 (1) (2011) 112–125.
- [39] S. Banumathy, R.K. Mandal, A.K. Singh, Structure of orthorhombic martensitic phase in binary Ti–Nb alloys, *J. Appl. Phys.* 106 (9) (2009), 093518.
- [40] M.H. Mueller, R.L. Hitterman, H.W. Knott, The atomic position parameter in alpha uranium-room temperature and above, *Acta Crystallogr.* 15 (1962) 421.
- [41] Y. Zheng, R.E.A. Williams, H.L. Fraser, Characterization of a previously unidentified ordered orthorhombic metastable phase in Ti–5Al–5Mo–5V–3Cr, *Scripta Mater.* 113 (2016) 202–205.
- [42] S. Banerjee, P. Mukhopadhyay, Kidlington, in: Phase Transformations: Examples from Titanium and Zirconium Alloys, vol. 12, Pergamon-Elsevier Science Ltd, 2007, pp. 1–813 in Phase Transformations: Examples from Titanium and Zirconium Alloys.
- [43] S. Bein, J. Béchet, Phase transformation kinetics and mechanisms in titanium alloys Ti–6.2.4.6, beta-CEZ and Ti–10.2.3, *J. Phys. IV* 6 (C1) (1996) 99–108.
- [44] M. Ikeda, Negative temperature dependence of electrical resistivity in Ti–Mo binary alloys, in: Proceedings of the 6th World Conference on Titanium, vol. I, 1988, pp. 313–318.
- [45] F. Sun, F. Prima, T. Gloriant, High-strength nanostructured Ti–12Mo alloy from ductile metastable beta state precursor, *Mater. Sci. Eng. A* 527 (16–17) (2010) 4262–4269.
- [46] J. Ho, E. Collings, Anomalous electrical resistivity in titanium–molybdenum alloys, *Phys. Rev. B* 6 (10) (1972) 3727–3739.

- [47] H.P. Ng, et al., Phase separation and formation of omega phase in the beta matrix of a Ti–V–Cu alloy, *Acta Mater.* 59 (8) (2011) 2981–2991.
- [48] F. Prima, P. Vermaut, G. Texier, D. Ansel, T. Gloriant, Evidence of  $\alpha$ -nanophase heterogeneous nucleation from  $\omega$  particles in a  $\beta$ -metastable Ti-based alloy by high-resolution electron microscopy, *Scripta Mater.* 54 (4) (2006) 645–648.
- [49] T. Duerig, G. Terlinde, J. Williams, Phase-transformations and tensile properties of Ti-10V-2Fe-3Al, *Metall. Trans A Phys Metall. Mater. Sci.* 11 (12) (1980) 1987–1998.
- [50] F. Bruneseaux, Apport de la diffraction des rayons X à haute énergie sur les transformations de phases, application aux alliages de titanes, Thèse de doctorat, Université de Lorraine, France, 2008.
- [51] A. Settefrati, E. Aeby-Gautier, B. Appolaire, M. Dehmas, G. Geandier, G. Khelifati, Low temperature transformation in the  $\beta$ -metastable Ti-5553 alloy, *Eur. Symp Marten. Transform.* 738–739 (2013) 97–102.
- [52] Y. Ohmori, T. Ogo, K. Nakai, S. Kobayashi, Effects of  $\omega$ -phase precipitation on  $\beta \rightarrow \alpha$ ,  $\alpha''$  transformations in a metastable  $\beta$  titanium alloy, *Mater. Sci. Eng. A* 312 (1–2) (2001) 182–188.
- [53] T. Li, D. Kent, G. Sha, J.M. Cairney, M.S. Dargusch, The role of  $\omega$  in the precipitation of  $\alpha$  in near- $\beta$  Ti alloys, *Scripta Mater.* 117 (Supplement C) (2016) 92–95.
- [54] S. Azimzadeh, H.J. Rack, Phase transformations in Ti-6.8Mo-4.5Fe-1.5Al, *Metall. Mater. Trans.* 29 (10) (1998) 2455–2467.
- [55] T.W. Duerig, J. Albrecht, D. Richter, P. Fischer, Formation and reversion of stress induced martensite in Ti-10V-2Fe-3Al, *Acta Metall.* 30 (12) (1982) 2161–2172.
- [56] P. Barriobero-Vila, V.B. Oliveira, S. Schwarz, T. Buslaps, G. Requena, Tracking the  $\alpha''$  martensite decomposition during continuous heating of a Ti-6Al-6V-2Sn alloy, *Acta Mater.* 135 (2017) 132–143.
- [57] A. Settefrati, B. Appolaire, E. Aeby-Gautier, Y. Le Bouar, G. Khelifati, Stress and strain fields calculations associated with the formation of intragranular alpha precipitates, in: *Proceedings of the 12th World Conference on Titanium*, 2012.
- [58] R. Shi, N. Ma, Y. Wang, Predicting equilibrium shape of precipitates as function of coherency state, *Acta Mater.* 60 (10) (2012) 4172–4184.
- [59] C. Angelier, S. Bein, J. Béchet, Building a continuous cooling transformation diagram of  $\beta$ -CEZ alloy by metallography and electrical resistivity measurements, *Metall. Mater. Trans.* 28 (12) (1997) 2467–2475.
- [60] E. Aeby-Gautier, et al., Isothermal  $\alpha''$  formation in  $\beta$  metastable titanium alloys, *J. Alloys. Compd.* 577 (Supplement 1) (2012) S439–S443.
- [61] B. Appolaire, A. Settefrati, E. Aeby-Gautier, Stress and strain fields associated with the formation of  $\alpha''$  in near- $\beta$  titanium alloys, *Mater. Today: Proc.* 2 (Supplement 3) (2015) S589–S592.
- [62] G. Charrier, et al., Study of the elemental partitioning for different transformations conditions in the Ti-5553 alloy, in: *Proceedings of the 13th World Conference on Titanium*, 2016, pp. 547–552.
- [63] A. Settefrati, et al., Precipitation sequences in beta metastable phase of Ti-5553 alloy during ageing, in: *Proceedings of the 12th World Conference on Titanium*, vol. 1, 2012.